Low-Cost Space Telescope Pointing Control System

J.R.Glaese,* H.F. Kennel,† G.S. Nurre,‡ S.M. Seltzer,§ and H.L. Shelton¶
NASA George C. Marshall Space Flight Center, Ala.

Vigorous efforts to reduce costs, coupled with changes in Space Telescope (ST, formerly LST) guidelines, took place in the fall of 1974. These events made possible a new design of the ST and its Pointing and Attitude Control System. The major design changes are summarized as : an annular Support Systems Module; removal of image motion compensation; reaction wheels instead of control moment gyroscopes; and a magnetic torquer system to perform the emergency and backup functions, eliminating the previously required mass expulsion system. Preliminary analysis indicates the Low Cost ST concept has met the newly defined requirements and results in a significantly reduced development cost.

Introduction

THE Space Telescope (ST) is to be a free-flying autonomous astronomical observatory that is to be launched in late 1982 by a Space Shuttle into a nominal 500-km circular orbit. The initial design, which was begun in 1971, was for a 3-m aperture telescope.[1] In the fall of 1974, the telescope aperture was changed to 2.4-m in order to reduce program costs. This paper describes a Pointing Control System (PCS) design for the Low Cost ST (LCST). While the requirements have not changed significantly with the decrease in aperture size, the configuration of the PCS is markedly different. A detailed comparison with prior designs, typified in Refs. 1 and 2, appears in a following paragraph. In general, the LCST design consolidates the necessary functions of the PCS among a minimum number of components and subsystems. The design, therefore, has been greatly simplified and made less costly; yet all aspects of the exacting performance specifications have been realized.

The requirements and guidelines to which the LCST PCS was designed are similar to those for the previous 3-m ST. The most important and most challenging requirement is the pointing stability of 0.005 arcsec (later changed to 0.007 arcsec) for durations up to 10 hr. This is the same number as was used for the 3-m ST, since the relatively small aperture change had a negligible effect on the pointing requirement. The maneuver requirement, specified as minimum time to rotate $\pi/2$ rad, was changed from 10 to 20 min. This change allowed considerable simplification and the possibility of using certain existing components. The final major requirement insures that the ST would be amenable to Shuttle retrieval in the event of a failure in the primary PCS.

PCS Description

Because of the vigorous effort to reduce cost and because of changes in the requirements and guidelines, the PCS for the LCST differs significantly from the previous 3-m design. These major changes consist of the deletion of some subsystems as well as changes in equipment.

A very important configuration change is the annular Support Systems Module (SSM). The choice of the 2.4 m aperture allows sufficient room between the Optical Telescope Assembly (OTA) and the Shuttle payload bay to permit the components that make up the SSM to be mounted in a "doughnut" arrangement around the circumference of the OTA near the primary mirror. In moving the SSM components nearer to the composite LCST center of mass, the two largest principal moments of inertia are reduced; consequently the required size of the momentum exchange controllers is reduced. A second change is the elimination of the Image Motion Compensation (IMC) system, which required movement of the telescope secondary mirror to correct image motion in order to achieve fine pointing. Preliminary studies performed under the LCST Advanced Technology and Development Program have shown that the pointing requirements can be achieved with a body-pointing system, wherein the entire spacecraft is moved to correct image motion.[2] Since a body-pointing system is required in either case, deletion of the IMC system reduces both the complexity and the cost of the PCS. The heart of the body-pointing system, the momentum exchange controllers, has also been changed for the LCST. Whereas single-gimbal control moment gyroscopes had been the baseline previously, the new design employs four reaction wheels (RW's) mounted in a skewed configuration. The reduced moments of inertia and the smaller maneuver requirement make possible the use of the High Energy Astronomical Observatory (HEAO) RW's with a modified motor. As in the initial ST design, magnetic torquers are used to control the angular momentum of the RW's. However, in the new design, the magnetic system also performs the emergency and backup functions in addition to momentum management. Since these functions previously were handled by mass expulsion jets, use of the magnetic torquers in this manner has allowed the elimination of this system. The configuration of the magnetic torquers has been changed in favor of a more efficient arrangement. Rather than the original six (three pairs of orthogonal torquers), the new design has four skewed torquers arranged in a fashion similar to that of the RW's. Thus, while redundancy has been maintained, the number of torquers has been reduced. Finally, maximum use has been made of HEAO and NASA standard components. A functional block diagram of the LCST is shown in Fig. 1.

The configuration of the LCST spacecraft is shown in Fig.2. Starlight enters the telescope from the left and is brought to focus behind the primary mirror where the scientific instruments are located.

The components of the PCS are located throughout the spacecraft. The sun sensors are mounted at either end of the telescope to permit each to view an unobstructed hemisphere. The four magnetic torquers are mounted around the circumference of the telescope forward of the SSM. Their dis-

Presented as Paper 75-1057 at the AIAA Guidance and Control Conference, Boston, Mass., Aug. 20-22, 1975; submitted Sept. 5, 1975; revision received Dec. 15, 1975.

Index categories: Earth Satellite Systems, Unmanned; Spacecraft Attitude Dymamics and Control.

*Applied Physicist, Pointing Control Systems Branch, Systems Dynamics Laboratory.

†Leader, Momentum Management Team, Pointing Control Systems Branch, Systems Dynamics Laboratory.

‡ST Lead Engineer, Control Systems Division, Systems Dynamics Laboratory. Member AIAA.

§Chief, Pointing Control Systems Branch, Systems Dynamics Laboratory. Associate Fellow AIAA.

¶Leader, Stabilization and Control Team, Pointing Control Systems Branch, Systems Dynamics Laboratory.

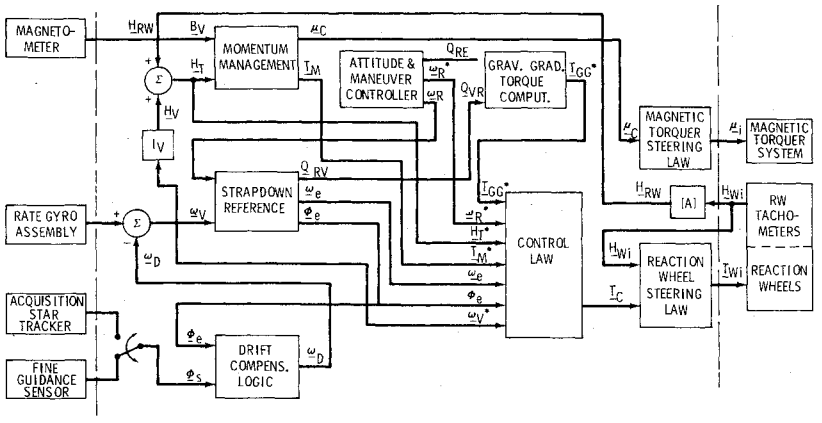

Fig. 1 LCST control system functional block diagram. Note: the necessity for the inclusion of the quantities with an asterisk has not yet been shown.

tance from the spacecraft center of mass, which is near the primary mirror, has been minimized to reduce the spacecraft moments of inertia. However, magnetic field contamination in the area of the scientific instruments constrains the choice of location. The three sets of primary sensors–the Fine Guidance Sensors (FGS's), The Reference Gyro Assembly (RGA), and the Acquisition Star Trackers (AST's)–are located on the focal plane assembly structure. This is the same structure that holds the scientific instruments. This arrangement insures long-term dimensional stability between these sensors. The magnetometer is located on the aft end of the spacecraft where internally induced magnetic fields are at a minimum. The RW's and digital computer are in the SSM.

PCS Design

The purpose of this activity was to determine the feasibility of meeting the pointing stability requirement of 0.005 arcsec in a body-pointing-only mode with RW's as actuators. A single-axis representation of the PCS was used in the analysis because of limitations on time and manpower (Fig. 3). The strapdown update gain (K_{up}) was assumed to be infinite in the following analysis; i.e., position error is solely from the FGS.

Preliminary Control System Synthesis

The purpose of this activity was to investigate bandwidth requirements for the body-pointing control system. The assumption was made (and supported by previous analysis) that the state feedback should consist of attitude rate, attitude, and integral of attitude, using gains K_R, K_P, K_I, respectively. Since a flexible body model of the LCST was not available, the criterion for selecting the optimum bandwidth was to minimize the line of sight (LOS) error due to sensor noise. The integral feedback was included to aid in reducing LOS errors due to static or near-static disturbances. The system in Fig. 3 can be made less sensitive to FGS noise and bandpass by updating at a low rate the strapdown system with FGS inputs. The final selection of gains and implementation will be defined to minimize the effects of such things as flexible structure, Rate Gyro (RG) noise, and RW vibrations.

Sensor and Actuator Noise Analyses

The approach to studying the effects of sensor and actuator noise was to minimize the rms pointing stability error in the presence of noise from the RG, and the FGS, and the torque noise from the RW's. The noise from each source was considered to be white, i.e., the Power Spectral Density (PSD) is constant. All noise inputs were assumed Gaussian with zero mean. The systems analyzed were assumed linear and continuous. To assess the pointing error (ϕ_e) for the noise inputs, the mean square value of the error was calculated by the equation

$$\Phi_e^2 = \sum_{i=1}^{n} (PSD_i/2\pi j) \int_{-j\infty}^{j\infty} |H(s)_i|^2 ds \qquad (1)$$

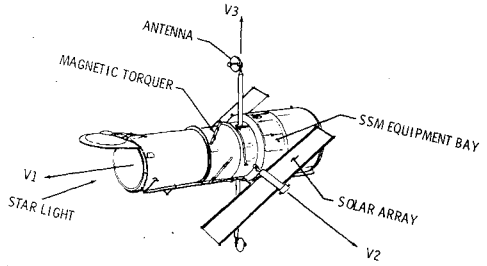

Fig. 2 Low-Cost Space Telescope.

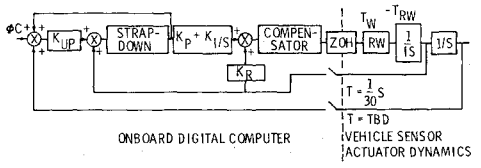

Fig.3 Single axis block diagram.

where the index i refers to the ith noise contributor, $H(s)_i$ is its transfer function, and n is the number of noise sources considered. The total mean squared pointing error for the concept studied is

$$\Phi_e^2 = \frac{PSD_{RG}K_R^2 + PSD_{FGS}(K_P^2 + K_I K_R) + PSD_{RW} \times 10^{12}}{2(K_P K_R - K_I I_V)} \qquad (2)$$

where I_V stands for the vehicle moment of inertia. The effect of noise from each source was studied separately and then collectively. The PSD for each noise source was varied about the "nominal" value, using the following ranges: rate gyro $= 6.0\text{x}10^{-5}$ to $2.4\ \text{x}10^{-4}$ $(\mu\text{rad/s})^2/\text{Hz}$ (Ref.3); FGS $= 2\text{x}10^{-6}$ to $1\text{x}10^{-4}$ $\mu\text{rad}^2/\text{Hz}$; RW $= 2\text{x}10\text{x}10^{-6}$ $(\text{N}\cdot\text{m})^2/\text{Hz}$ (Ref.4). Figure 4 is a portrayal of pointing stability error vs control system bandwidth for a given rate gyro noise input with the FGS noise varied and no RW noise. Allowing 0.005-μrad rms of the 0.025-μrad requirements to be budgeted to sensor noise, Fig. 4 shows that the bandwith should be approximately 1.0 Hz. This is achieved by setting gains as follows: $K_I = 7.3\text{x}10^5$ N·m/rad·sec, $K_p = 1.7\text{x}10^6$ N·m/rad, $K_R = 3.7\text{x}10^5$ N·m·sec/rad.

Reaction Wheel Model Development

Because of the stringent pointing requirements, it became evident that the small signal nonlinearities in the RW must be considered. The nonlinearity felt to be most significant was the bearing friction in the rotor bearints. The bearing friction was modeled as the solid friction model.[5] Figure 5 shows the model for an individual RW where its output ($-T_{RW}$) is the torque applied to the spacecraft.

The approach to assessing the effects of bearing friction was to consider, for the planar model, two RW's with their spin axes aligned in a plane perpendicular to the minimum

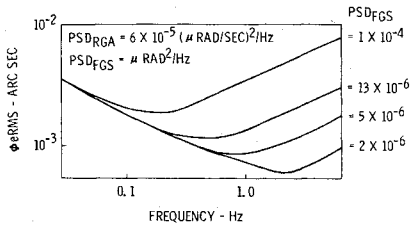

Fig.4 Sensor noise analysis.

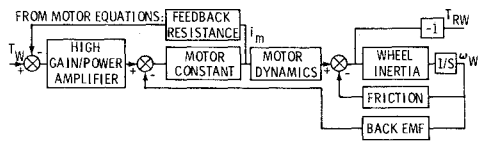

Fig.5 Reaction wheel model. Power/high gain amplifier (K_A) = 10,000 $V/V/S$. Feedback resistance (R_F) = 0.484 ohms. Motor time constant (K_T) = 0.002 sec. Motor constant (K_M) = 0.484 N-m/amp. Wheel inertia (I_W) = 0.2 kg·m.^{2} Back emf (K_B) = 0.484 V/rad/sec. Friction = Dahl Model.

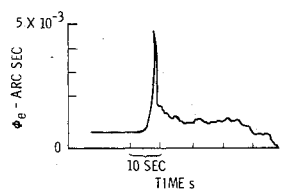

Fig.6 Pointing error due to one RW passing thru zero rate.

inertia axis of the spacecraft. For the "nominal" RW friction parameters [$\gamma = 5\text{x}10^3$ (N·m·rad)$^{-1}$ and $T_{gfo} = 0.0424$ N·m] the peak pointing errors were determined for both cases mentioned. The analysis is similar to the approach reported in Refs. 6 and 7. The pointing error is caused by an error between the torque command and the torque resulting from an RW passing through zero speed. Figure 6 shows the response for one wheel passing through zero speed. When one wheel passes through zero speed the peak LOS transient error is 0.005 arcsec; when two wheels pass through zero speed simultaneously, it is 0.015 arcsec. While one wheel may pass through zero speed frequently, the likelihood of two wheels passing through zero speed simultaneously is very low, and the peak pointing error for the latter is not considered a problem. For example, when this peak error is averaged over a time period commensurate with experiment observation duration, its effect on the rms pointing error becomes small.

The next aspect to be considered is the system sensitivity of variations in the solid friction parameters (γ and T_{gfo}). The approach taken was to investigate the existence of limit cycles via describing funciton analysis. The describing function was then verified by simulation. The describing function (N) used for the solid friction nonlinearity was that developed in Ref. 6. The plant and controller are modeled as a continuous system to which a zero order hold has been added to represent the sampled data characteristics of the onboard digital computer. The RW transfer function is

$$G(s) = \frac{(2I_V s^5 + 2I_V s^4/T_M + 2KI_V s^3 + K_R K s^2 + K_p K s + K_I K)\ (1 - e^{-Ts})}{2I_W T s^3\,(I_V s^5 + I_V s^4/T_M + KI_V s^3 + K_R K s^2 + K_p K s + K_I K)} \tag{3}$$

where $K = K_A R_F / R_T R_M$ (see Fig. 5 for definitions of these terms). The Nichols chart showing the linear transfer function and the describing function of one RW operating about zero speed is shown in Fig. 7. The figure shows that when $(1/N)$ $\gamma(T_{gfo})^2 = 5000$, a stable limit cycle will exist. Outside the range shown on Fig. 7, it may be shown that unstable limit cycles can exist. Simulation results confirm the predicted stable limit cycle characteristics. By observing the simulation

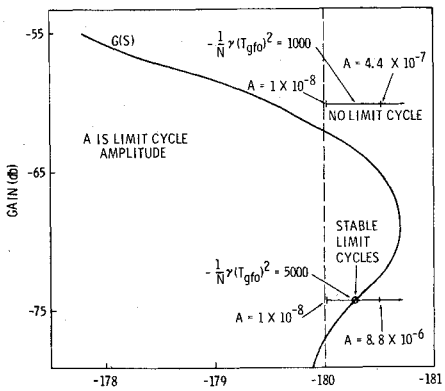

Fig.7 Nichols chart.

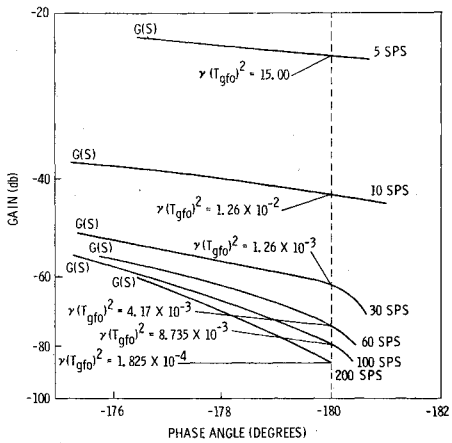

Fig.8 Nichols chart showing sampling effects.

results for several limit cycle conditions, it was observed that the LOS pointing error is always negligible relative to the pointing stability requirement of 0.005 arcsec. Presently, analysis is under way to investigate the discrete case by applying the discrete describing function.[8] Preliminary results of this analysis are depicted in Fig. 8. The figure defines the minimum value of $\gamma(T_{gfo})^2$ vs sample rate for which limit cycles will occur.

Digital Effects

Variations in sample rates from 5 to 100 samples per second were applied to the body control system while minimizing quantization effects. There was no significant change in body-pointing error Φ_e due to sample rate variations over the entire range of study if the phase lag associated with the sample-and-hold is compensated. Analysis shows that Φ_e is approximately $0.6\text{x}10^{-4}$ arcsec for all sample rates greater than five samples per second.

The effect of quantization on pointing stability has been assessed on a hybrid simulation. Quantization as used herein is the resolution to which each sensor must be read into the onboard digital computer. In the case of torque, quantization refers to the accuracy that one must be able to command the RW and expect a reasonable response. The quantization ranges studied for both sensors and RW's were FGS (q_{fgs}): 3.75×10^{-5} to 0.024 arcsec; RG(q_{rg}): 0.0075 to 0.024 arcsec/sec; torque (q_{trw}): 7.5×10^{-5} to 0.024 N·m. Each quantizer was studied individually to set the minimum level that resulted in a system error of approximately 0.001 arcsec. The rms error due to the combined effect of all three quantizers is

0.0017 arcsec. The results of this analysis showed that the following quantization levels are desiragle: $q_{fgs}=0.003$ arcsec, $q_{rg}=0.003$ arcsec/s, and $q_{trw}=0.003$ N·m.

Pointing Stability Error Budget

As previously stated, the purpose of the entire PCS design acitvity is to determine the feasibility of achieving the 0.005-arcsec pointing stability requirement. The RSS of the pointing stability errors caused by quantization, FGS noise, RGA noise, and torque noise is 0.0027 arcsec.

The RSS of the requirement less the RSS of 0.0027 arcsec is 0.0042 arcsec.This 0.0042 arcsec presently is reserved for other disturbances that have not yet been assessed. The following disturbances contribute to the pointing stability budget, none of which has yet been analyzed for the LCST: appendage motion, recorder dynamics, experiment operation, flexible body effects, and RW imbalance. RW imbalance is expected to be the most severe of those disturbances not yet analyzed.

Attitude Reference, Maneuvers, and Momentum Management

Attitude Reference and Maneuvers

The level of precision required for the ST leads to the choice of RWs as primary controllers. They require, however, some means of preventing excessive angular momentum buildup. The desire for long life, high reliability, and low contamination leads to the selection of magnetic torquers as auxiliary actuators for momentum management. These auxiliary actuators can also provide backup to the primary controllers in case of failures. By very simple analog loops the torquers can be used in a rate damping mode to drive the vehicle to a gravity gradient stable local vertical attitude to await subsequent servicing or recovery by the Shuttle. For this reason, a reaction control system was considered unnecessary and was eliminated from the design, allowing significant cost reduction.

For vehicle attitude determination, three coordinate frames are of primary interest: inertial frame E, vehicle fixed frame V, and moveable reference frame R (the frame R represents the commanded attitude of the V frame). For overall system simplicity, strapdown integration is done in terms of relative four parameter (quaternion Q_{VR}) attitude variables, as in Eq. (4). This offers the following advantages: 1) a single algorithm for all attitude control modes (fine pointing, maneuvering, etc.); 2) small vehicle attitude errors at all times; 3) continuous updating of the strapdown calculation (if a suitable position sensor is available) through a drift rate correction added to the reference frame rate; and 4) easy shaping of maneuver, scan, or other rate profiles. According to a theorem by Euler, any direction cosine matrix such as $[VR]$ can be expressed as a single rotation through an angle Φ_e about an axis represented by a unit vector u_e.[9] The corresponding quaternion has four components: $Q_{VR}=[\sin(\Phi_e/2)u_e, \cos(\Phi_e/2)]^T$. If ω_V and ω_R represent the inertial angular velocities of the V and R frames resolved respectively into these frames, the relative quaternion Q_{VR} may be determined by integrating the expression

$$\begin{bmatrix}\dot{Q}_{VR1}\\ \dot{Q}_{VR2}\\ \dot{Q}_{VR3}\\ \dot{Q}_{VR4}\end{bmatrix}=\tfrac{1}{2}\begin{bmatrix}0 & (\omega_{V3}+\omega_{R3}) & -(\omega_{V2}+\omega_{R2}) & (\omega_{V1}-\omega_{R1})\\ -(\omega_{V3}+\omega_{R3}) & 0 & (\omega_{V1}+\omega_{R1}) & (\omega_{V2}-\omega_{R2})\\ (\omega_{V2}+\omega_{R2}) & -(\omega_{V1}+\omega_{R1}) & 0 & (\omega_{V3}-\omega_{R3})\\ -(\omega_{V1}-\omega_{R1}) & -(\omega_{V2}-\omega_{R2}) & -(\omega_{V3}-\omega_{R3}) & 0\end{bmatrix}\begin{bmatrix}Q_{VR1}\\ Q_{VR2}\\ Q_{VR3}\\ Q_{VR4}\end{bmatrix} \tag{4}$$

The rate ω_V is measured by rate sensors on the vehicle or computed from measured attitudes. The rate ω_R is commanded in whatever manner is required to produce the desired motion, including inertial hold where ω_R is set to zero. The vehicle pointing error ϕ_e is defined as $\phi_e=\Phi_e u_e\approx 2[Q_{VR1}, Q_{VR2}, Q_{VR3}]^T$. The corresponding rate error is $\omega_e=\omega_V-\omega_R$.

The feedback control torque T_F is developed from these errors and will cause the vehicle to track the motion of the reference frame R

$$T_F=I_V(A_I\int \phi_e dt+A_p\phi_e+A_R\omega_V-\omega_R)$$

where I_V is the estimated vehicle inertia. For convenience we let $K_I=I_VA_I$, $K_p=I_VA_p$, $K_R=I_VA_R$.

The total control torque command T_c may include terms other than those containing state feedback. These additional terms would compenstate for known disturbance torques such as those due to gravity gradient or vehicle maneuvers; however, the performance improvements versus additional complexity and software must be assessed. A candidate control algorithm is

$$T_C=I_V\dot{\omega}_R+\omega_V\times H_T-T_{GG}-T_M-T_F \tag{5}$$

where $I_V\dot{\omega}_R$ is the maneuver torque command, $\omega_V\times H_T$ is the gyroscopic torque, T_{GG} is the gravity gradient torque, and T_M is the magnetic torque. The maneuver term $I_M\dot{\omega}_R$ is computed at the same time as ω_R and shapes the maneuver velocity profile according to predetermined requirements. The total angular momentum H_T of the system, including both vehicle momentum and total RW system momentum H_{RW}, is $H_T=H_{RW}+I_V\omega_V$. A trapezoidal maneuver rate profile was assumed. The area under the maneuver profile curve is the maneuver angle. The profiles are easily modified to round the corners of the acceleration curve to reduce the disturbances that tend to excite the flexible body dynamics. Since the velocity ω_V is determined by measurement, it includes errors. The numerical integration of Eq. (4) also introduces errors. The combined effect of these discrepancies is known as drift. When an attitude sensor (AST or FGS) output is available, it will be used to correct for this drift.

Momentum Management

The magnetic actuators will consist of electromagnets in which the dipole moment produced is proportional to the current flowing through the magnet windings. This current is the controlled quantity used to produce a desired dipole moment and, hence, torque. The configuration of electromagnets selected for the LCST magnetic torquer system (MTS) consists of four torquers mounted in a skewed fashion. If the dipole moment of the ith torquer is μ_i, the total dipole moment M is

$$M=\begin{bmatrix}S & S & S & S\\ C & -C & -C & C\\ C & C & -C & -C\end{bmatrix}\begin{bmatrix}\mu_1\\ \mu_2\\ \mu_3\\ \mu_4\end{bmatrix}=A_{MT}\mu \tag{6}$$

The constants S and C are defined as $S=\sin\lambda$; $C=(\cos\lambda)/\sqrt{2}$. The angle λ represents the torquer elevation out of the V2-V3 plane and has been selected as $\lambda=35.26°$ for maximum symmetry and most spherical volume. This con-

figuration allows failure of a coil without restricting attitude capability. Failure of two coils severely restricts the attitudes where momentum containment is still achievable. Only those attitudes would be allowed where the magnetic field B lies generally along the normal to the plane defined by the active torquers.

The torque of interaction of the MTS dipole moment M with the geomagnetic field B is $T_M = M \times B$. From this equation it can be seen that no torque can be generated along the direction parallel to B. This is a fundamental limitation of the MTS, eliminating it as a candidate for primary control actuators. The rate of change of the total angular momentum $\dot{H}_T$ is equal to the sum of the disturbance torques on the vehicle: $\dot{H}_T = T_E + T_M$, where T_E is the sum of all disturbance torques excluding the magnetic torque T_M from the MTS. It is desired that on the average the sum of the magnetic torques and the disturbance torque be zero; accomplishing this is the basic task of the MTS and associated logic.

The total momentum H_T represents the integrated effect of all torques acting on the LCST spacecraft; this is the best estimate of the momentum error from a desired bias momentum H_B. Because of the previously discussed limitations of the MTS, the momentum error $H_D = H_T - H_B$ cannot be reduced to zero in an arbitrarily short time. Thus, the length of time required to reduce the momentum error H_D to a negligible level will depend on: 1) the available dipole moment capability; 2) the variations in B; and 3) the desaturation command law. The simplest law currently under consideration is the "cross product law" (CPL) defined by $M_C = -K_M H_D \times B/B^2$; where M_C is the dipole moment command to the MTS and K_M is a gain. This law produces a torque proportional to the component of H_D normal to B.

The principal advantage of the CPL is simplicity. The disadvantages of the CPL are: 1) momentum desaturation is done inefficiently, increasing MTS size requirements; 2) the inability to accurately predict the RW momentum several orbits in advance forces a reduction in the momentum considered safely available, thus reducing maneuver rates; 3) large dipole commands increase power requirements and increase potential for magnetic contamination, and generally increase power requirements for the RW system. Because of these disadvantages, more precise alternatives to the CPL become desirable.

The dipole moment produced by a magnetic torquer will be proportional to current through its coils. Thus, the power dissipated as heat by MTS is proportional to $\mu^T \mu$ (the torquers are assumed to be identical). The total energy consumed by the MTS is proportional to the function Ψ

$$\Psi = \int_o^{T_D} \mu^T \mu / 2 dt \tag{7}$$

The Minimum Energy Desaturation Law (MEDL) is developed by minimizing the function Ψ while enforcing a constraint on the integral of the magnetic torque T_M

$$H_D = \int_o^{T_D} T_M dt = -\int_o^{T_D} \tilde{B}\, \mu dt$$

$$\text{where } \tilde{B} = \begin{bmatrix} 0 & -B_3 & B_2 \\ B_3 & 0 & -B_1 \\ -B_2 & B_1 & 0 \end{bmatrix} \tag{8}$$

Using the Lagrange multiplier approach, a new function ν is defined

$$\nu = \Psi + Y^T \left(\int_o^{T_D} \tilde{B}\, \mu dt - H_D \right) \tag{9}$$

where Y is a constant vector of Lagrange multipliers. The condition for minimization is $\delta \nu = 0$. This condition leads to

$$\mu = A_{MT}^T \tilde{B} Y \tag{10}$$

If Eqs. (6) and (8) are employed, the vector Y can be determined as

$$Y^T = C_M^{-1} H_D$$

where

$$C_M = \int_o^{T_D} \tilde{B} A_{MT} A_{MT}^T \tilde{B} dt \tag{11}$$

Equations (10) and (11) summarize the MEDL. The integral C_M is evaluated using a math model of the geomagnetic field. Since C_M must be inverted, it must be nonsingular. This is easily shown to be true as long as the geomagnetic field B varies in direction over the desaturation interval (0, T_D). The period T_D was set at half an orbital period in order to include the major variations in B and to be compatible with the period of gravity gradient disturbances.

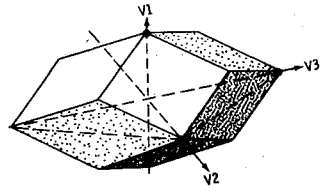

Fig.9 Maximum momentum envelope (4 RW's).

Reaction Wheel Control

Mounting Arrangement

Four RW's are used to allow for the failure of one. They are mounted similar to the HEAO-B RW's, but with a polarity definition such that any RW can be mounted at any of the RW positions without the need for different mounting hardware or change in polarity definitions. The transformation from RW momentum scalars (H_{Wi} for the ith RW) to total RW system momentum H_{RW} is

$$H_{RW} = [H_{RW1},\ H_{RW2},\ H_{RW3}]^T$$
$$= A_{RW} [H_{W1},\ H_{W2},\ H_{W3},\ H_{W4},]^T \tag{12}$$

with the transformation matrix A_{RW} being

$$A_{RW} = \begin{bmatrix} +S & -S & +S & -S \\ -C & -C & +C & +C \\ -C & -C & -C & -C \end{bmatrix}$$

where S and C are as previously defined, but with $\lambda = 20$ deg. Since the angular momentum changes (which are equivalent to the RW torque) are also along the wheel axes, the total torque on the RW system is $T_{RW} = [T_{RW1},\ T_{RW2},\ T_{RW3}]^T = A_{RW} T_W$ where the torque on the ith RW is $T_{Wi} = \dot{H}_{Wi}$ and $T_W = [T_{W1},\ T_{W2},\ T_{W3}]^T$. The elevation (or depression) angle of 20 deg gives a ratio of maximum $V2$ or $V3$ momentum to maximum $V1$ momentum of $2.7H$ to $1.4H$ or 0.52, where H is the maximum achievable wheel momentum. The ratio of minimum to maximum vehicle inertia is 0.4. This gives 27% more maneuvering capability about the $V1$ axis than about the $V2$ or $V3$ axis. The maximum momentum envelope for four wheels is shown in Fig. 9.

Steering Law with Distribution and Failure Accommodation

The RW steering law is derived from the pseudo-inverse $A_{RW}^{\dagger}$ of the matrix A_{RW}, where $A_{RW}^{\dagger} = A_{RW}^T (A_{RW} A_{RW}^T)^{-1}$

and an arbitrary scalar T_Δ (which signifies the one remaining degree of freedom)

$$T_W = A_{RW}^{\dagger}[T_{C1}, T_{C2}, T_{C3}]^T + [T_\Delta, -T_\Delta, -T_\Delta, T_\Delta]^T \quad (13)$$

The scalar T_Δ can be used to achieve a desirable RW momentum distribution as long as no wheel has failed or is saturated. Also, it can be used to zero the torque command to a failed wheel, thus avoiding the need for four more steering law inverses to cover the failure of any wheel.

For four wheels, there are several reasonable momentum distributions. One distribution which at saturation conforms to the maximum momentum envelope and is simple to implement is

$$T_\Delta = K_\Delta [(H_{W3} - H_{W4})H_{1A} - (H_{W1} - H_{W2})H_{1B}] / [2(H_A + H_{1B})] \quad (14)$$

where $H_{1A} = 2H - |H_W + H_{W2}|$ and $H_B = 2H - |H_{W3} + H_{W4}|$ are the maximum combined angular momentum capabilities of pairs A (RW#1 and RW#2) and B (RW#3 and RW#4) along the $V1$ axis; K_Δ is the inverse of the time constant. When T_Δ is zero, the same percentage of the $V1$ momentum capability is used by each pair: $(H_{W1} - H_{W2})/H_{1A} = (H_{W2} - H_{W4})/H_{1B}$.

Momentum, Power, and Torque Requirements

To assess the RW system requirements, the following vehicle and orbital data were used: principal inertias, $I_1 = 17\ 360\ \text{kg}\cdot\text{m}^2$, $I_2 = 42\ 950\ \text{kg}\cdot\text{m}^2$, $I_3 = 41\ 780\ \text{kg}\cdot\text{m}^2$; maximum gravity gradient torque $= 0.047\ \text{N}\cdot\text{m}$; cyclic momentum peaks $= 20\ \text{N}\cdot\text{m}\cdot\text{sec}$. A trapezoidal maneuver profile was assumed. A 90° maneuver in 18 min (20 min minus 2 min settling time) requires the following numerical values: maximum maneuver rate: 0.111°/sec; maximum maneuver torque $= 0.309\ \text{N}\cdot\text{m}$; maximum momentum change $= 83.28\ \text{N}\cdot\text{m}\cdot\text{sec}$; maximum power $= 72.88$ W. There is a definite possibility that the maximum gravity gradient torque (0.05 N·m), the maximum maneuver torque (0.31 N·m), and the maximum magnetic torque (0.2 N·m) occur simultaneously and add. Therefore, a maximum RW torque of 0.5 N·m (per wheel) has been selected, giving a safety factor of 1.7 for all wheels operational; however, the maximum torque available for the worst direction maneuver will drop to 0.47 N·m if one wheel fails.

There are three reasons why the HEAO RW motor should be replaced: 1) an AC motor is very nonlinear, 2) the HEAO motor can produce only 0.2 N·m maximum torque, and 3) top speed is only 200 rad/sed. The minimum dimensions of the angular momentum envelope (Fig. 9) for four RW's are $H_1 = 82\ \text{N}\cdot\text{m}\cdot\text{sec}$, $H_2 = H_3 = 113\ \text{N}\cdot\text{m}\cdot\text{sec}$. This envelope can accommodate the maneuver momentum change (83 N·m·sec) on top of the cyclic momentum peak (20 N·m·sec). When the cyclic momentum is not centered and the momentum change to accommodate the magnetic desaturation adds to the total, not enough maneuver momentum is available for the required 90° maneuver in 18-min time duration. The failure of a RW reduces the momentum envelope drastically (by 75%). While full attitude control can be maintained, the maneuvering capability is severely reduced.

The following RW design values are proposed: maximum angular momentum $= 60\ \text{N}\cdot\text{m}\cdot\text{sec}$; wheel inertia $= 0.2\ \text{kg}\cdot\text{m}^2$; no load speed $= 300$ rad/sec; maximum torque capability $= 0.5\ \text{N}\cdot\text{m}$; stall torque (design only) $= 5\ \text{N}\cdot\text{m}$. Since the average power allocation for the entire PCS is at present only 150 W (250-W peak), every effort should be made to recover negative power, i.e., to retrieve during deceleration the energy stored in the RW's.

Conclusions

The work reported in this paper had as its purpose the development of a PCS concept for the LCST that would have the lowest development and fabrication cost consistent with the study requirements. Preliminary results indicate that the resulting concept has achieved this purpose. In each case where a change has been made from the original 3-m design, a cost savings has been realized.

References

[1] Program Development: "Large Space Telescope Phase A Final Report," TM S-64726, NASA, Dec. 1972.

[2] Rybak, S. C., "Fine Pointing Control System for Large Space Telescope," NASA Contract NAS8-28983, March 1974.

[3] Harris, R. et al., "Spectral Density Measurements of Gyro Noise," E-2641, Charles Stark Draper Laboratory, Cambridge, Mass., Feb. 1972.

[4] Chiarappa, D. J., "Evaluation of Control Systems for Fine Pointing of Astronomy Spacecraft to 0.025 urad (0.005 arcsec)," General Dynamics Convair, San Diego, Calif. CASD-ERR-73-006, Dec. 1973.

[5] Dahl, P. R., "A Solid Friction Model," The Aerospace Corp., El Segundo, Calif. TOR-158 (3107-18), May 1968.

[6] Kuo, B. C., Seltzer, S. M. and Singh, G., "Limit Cycle Analysis of Large Space Telescope with CMG Nonlinearity," *Journal of Spacecraft and Rockets*, Vol. 12, Aug. 1975, pp. 472-476.

[7] Seltzer, S. M., "Large Space Telescope Oscillations Induced by CMG Friction," *Journal of Spacecraft and Rockets,* Vol. 12, Feb. 1975, pp. 96-105.

[8] Kuo, B. C. and Singh, G., "Continuous and Discrete Describing Function Analysis of the LST System," NASA Contract NAS8-29853, Jan. 1974, pp. 90-121.

[9] Goldstein, H., 1950: *Classical Mechanics,* Addison Wesley, Reading, Mass., p.118.